J. Fluid Mech. (1996), *vol.* 327, *pp.* 373–392

An energy model for artificially generated bubbles in liquids

By F. AITKEN, F. M. J. McCLUSKEY† AND A. DENAT

Laboratoire d'Electrostatique et des Matériaux Diélectriques,
Centre National de la Recherche Scientifique, 38000 Grenoble, France

(Received 6 February 1995 and in revised form 22 May 1996)

A mathematical analysis is carried out to model the series of processes following the occurrence of an electron avalanche in a liquid right through to the emission of a pressure transient and the formation of a bubble. The initial energy distribution is chosen to be Gaussian and it is assumed that the electrical energy injected into the system is transformed into thermal and mechanical components. From the mechanical point of view, an outgoing spherical pressure transient is formed at the edge of the plasma region, and at a later time a bubble is also formed. Theoretically, the pressure transient accounts for about 15% of the total injected energy, while it is necessary to revert to experimental results to fix the energy associated with the bubble (about 2%). A minimum such value can, however, be estimated. The maximum pressure amplitude is calculated. Concerning the thermal component of the energy, some is absorbed as internal energy by the liquid, while the remainder is stocked as latent heat of vaporization. The maximum temperature difference is derived as are the different energies as functions of the total injected energy. The advantage of this type of model is that the gas/vapour temperature in the bubble can continue to rise after the phase change takes place. The maximum bubble size following a given energy injection is calculated assuming an adiabatic expansion process. A mathematical expression for the liquid flow induced by the outgoing pressure transient is also found. Comparison between experimental and theoretical results is particularly good.

1. Introduction

The first major published study of cavitation and bubble dynamics was undertaken by Besant (1859), with an analytical treatment carried out by Rayleigh (1917). Although this was a particularly simple model for spherical bubble collapse, it gave remarkedly good results and still forms the basis of today's bubble dynamics research. The subject has since advanced to the point where the conditions of cavitation onset are predictable as well as the subsequent effects on both the liquid and any nearby boundaries. The phenomenon is observable in any liquid where a phase change may occur due to variations in the pressure field. The domain of application is clearly very large, for example in ophthalmology, chemical reactors, hydraulic and electrical machinery, ultrasound transducers and of course underwater propellers. An extensive review of the cavitation bubble has recently been published with a wide ranging and complete bibliography (Leighton 1994).

Depending on the field of interest, the effects of cavitation can be either destructive or beneficial. Cavitation bubbles generated near a solid surface will, eventually,

† Present address: Department of Mechanical Engineering, University of Brighton, Moulsecoomb, Brighton BN2 4GJ, UK.

seriously erode matter from that surface (see, for example, Knapp, Daily & Hammitt 1970; Pearsall 1972; Wheeler 1960; Hammitt 1966, 1980). In sonochemistry, bubbles may play the role of a catalyst by favouring certain chemical reactions, while in lythotripsy, kidney stones and gall stones can be broken up (Kitayama *et al.* 1987; Coleman *et al.* 1987; Coleman & Saunders 1989; Delius *et al.* 1988; Vakil, Gracewski & Everbach 1991; Philipp *et al.* 1993). The appearance of naturally generated cavitation bubbles is still random in space and time and thus their study can be very time consuming. Artificially generated bubbles are therefore the best means of repeatable data collection.

Many experimental techniques have been developed to this end, including the use of electrical breakdown of liquids (Harrison 1952; Naude & Ellis 1961), but the most important one is the optical breakdown of liquids (see, for example Lauterborn 1972; Vogel & Lauterborn 1988; Hentchel & Lauterborn 1982; Alloncle *et al.* 1990; Alloncle, Dufresne & Autric 1993; Sacchi 1991). This involves focusing an intense beam of laser light at a fixed point in the liquid. Breakdown occurs at the focal point. Another means of repeatedly generating bubbles of a given size involves the application of an electric field between a point and a planar electrode (Kattan, Denat & Lesaint 1989; Kattan, Denat & Bonifaci 1991). The observation of current impulses indicates the occurrence of electron avalanches at the point and thus the formation of a bubble there as a consequence. In the case of laser breakdown, bubble sizes range typically from a few hundred microns to several millimetres, while in the second case from a few microns to a few hundred microns, depending on the energy absorbed by the liquid. In both cases, the bubble appearance is linked to the formation of a 'micro-plasma' and the emission of pressure transients.

There is to date in the literature no available analysis of the transformation of the initial injected energy forming the plasma into the thermal and mechanical energies relevant to the formation of a bubble. The aim here is to develop such a model, linking in a formal way the pressure transient amplitude, the liquid and vapour temperatures and the maximum bubble size, etc., to the injected energy. In this energy model, a number of reasonable approximations, e.g., concerning the plasma, need to be made since certain quantities are not directly measurable.

Therefore, in order to carry out as complete a theoretical study as possible of the phenomena observed in artificial bubble generation applicable to both laser breakdown of liquids and formation due to electrical current impulses, the analysis must begin with consideration of the energy W_i injected into the system and how it evolves, i.e. the formation of a cold plasma in the liquid and the subsequent appearance of a pressure wave and a bubble. It is known from experimental evidence that most of the energy W_i (about 80%) serves to heat the liquid while most of what remains is dissipated by the emitted pressure wave (Vogel & Lauterborn 1988; Vogel, Lauterborn & Timm 1989). For a realistic account of events, the dynamics of the bubble itself must then be considered in relation to its position behind the outgoing pressure wave. Since full access to the data concerning electrically generated bubbles as well as the conditions under which the experiments were carried out is available, the analysis is based on those experiments. However, the resulting expressions should apply to laser breakdown phenomena.

The assumptions made in the analysis are stated followed by mathematical treatment of the energy injection and its transformation into thermal and mechanical components. In as much as is possible the chronological order of the observed experimental events will be followed.

2. Formulation of the model

2.1. *Assumptions*

The energy injection takes the form of an electron avalanche in the liquid phase, giving rise to a spherical volume containing separated electrical charges (positive ions and electrons). The dimensions of this plasma zone are generally of the order of the radius of curvature of the point (Hernandez-Avila, Bonifaci & Denat 1994). It is referred to as a localized non-equilibrium plasma. Its radius is r_0 with its centre defined as $r = 0$. It is further supposed that at that particular point the pressure and temperature rise almost instantaneously from (T_∞, P_∞) to (T_{m0}, P_{m0}) at the moment of energy deposition. The values (T_{m0}, P_{m0}) are also assumed to be much greater than the critical values (T_c, P_c). The injected energy is assumed to break up into thermal components (internal and heating) and mechanical components (bubble and pressure transient).

2.2. *The initial energy distribution in the plasma*

In the short time it takes for the plasma to form ($\approx 10^{-12}$ s) no density or volume change can occur. Consequently the local temperature T rises dramatically with a corresponding rise in pressure P. It is also supposed that for $r > r_0$, the initial radius of the plasma, the temperature and pressure are as yet unchanged from ambient values. Experimental data on either distribution are particularly difficult to obtain and the reasonable assumption that they are Gaussian is made. This is generally taken to be the case in laser breakdown (Docchio *et al.* 1988). Thus, the distribution $g(r)$ is written

$$g(r) = \frac{P(r) - P_\infty}{P_{m0} - P_\infty} = \frac{T(r) - T_\infty}{T_{m0} - T_\infty} = \frac{\exp(-r^2/2\sigma^2) - \exp(-r_0^2/2\sigma^2)}{1 - \exp(-r_0^2/2\sigma^2)} \tag{1}$$

for $r \in [0, r_0]$. Here, P_∞ is the undisturbed applied hydrostatic pressure and P_{m0} the maximum initial pressure value at the plasma centre, σ is the Gaussian standard deviation. It has been chosen to be the same for both temperature and pressure. This is usual when dealing with gases, but care must be taken in the case of liquids. This point will be discussed later. It is appropriate here to relate the plasma volume in some physical way with the initial size of the bubble. This will help in the definition of the initial conditions for the bubble growth.

In the pressure phase diagram shown on figure 1, the distribution of pressure from the plasma centre ($r = 0$) outwards to $r = r_0$ is graphically represented. This is a straight line making an angle α with the horizontal axis and is given by

$$\tan\alpha = \frac{P_{m0} - P_\infty}{T_{m0} - T_\infty}. \tag{2a}$$

There is a lower limit on the value that α can take, denoted α_l, where

$$\tan\alpha_l = \frac{P_c - P_\infty}{T_c - T_\infty}. \tag{2b}$$

Both the pressure and temperature at the centre are considered to be well above the critical values and, as represented in figure 1, it is assumed that the pressure–vapour curve is not crossed. If it were crossed, an interface would appear at the radius corresponding to the point of crossover. Thus, there would be a significant quantity of injected energy lost to heating the surrounding liquid. This is assumed not to be the case and the initial bubble formation involves the entire plasma region of radius r_0.

With the qualitative assumption of Gaussian distribution of temperature and pressure, some means of quantitatively evaluating both of these must be defined,

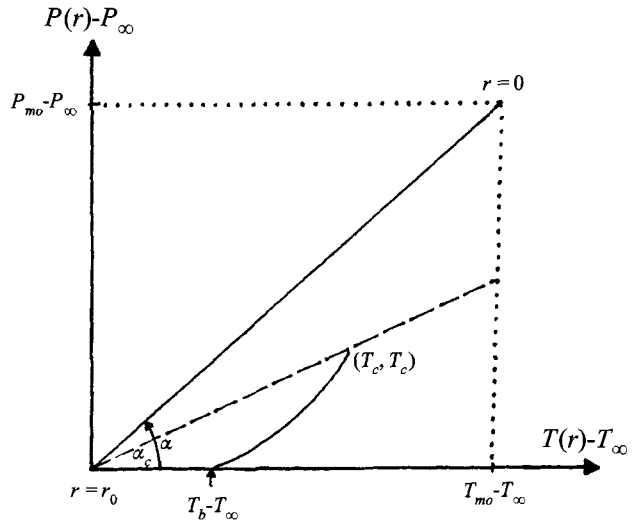

FIGURE 1. Schematic diagram of the radial variation of the plasma state (solid line) for Gaussian distributions of temperature and pressure (see equation (2*a*)). The dashed line represents the lowest limit the distribution can have (equation (2*b*)). Scales are arbitrary. T_b is the boiling temperature at P_∞.

relating them to the total injected energy. To this end, the energy is supposed divided into two components: thermal energy (E_T) to bring the temperature from T_∞ to T_{m0} and mechanical energy (E_P) to change the pressure from P_∞ to P_{m0}, with Gaussian distributions about these centre-point values. If W_i is the total injected energy, then

$$W_i = E_T + E_P. \tag{3}$$

Energy losses to light emission are ignored (Vogel & Lauterborn 1988). Experimentally, between 10% and 20% of the injected energy is typically lost to an initial pressure transient, less than 5% to the bubble and the remaining 80% or so is transformed into heat. It is among our intentions to physically justify these orders of magnitude.

Before determining the two energy components in (3), it is necessary to discuss the formation of the pressure transient from the initial Gaussian pressure distribution in the plasma. From the centre out, a pressure wave is emitted, whose velocity of propagation is a direct function of the pressure at any given point; the higher the pressure, the greater the velocity of sound. The emitted pressure waves will therefore 'catch up' with each other to form an unsteady pressure front (Osborne & Taylor 1946).

For simplicity, it is assumed that this redistribution of pressure occurs without energy loss, and that the initial maximum amplitude on the pressure transient front, formed at a distance, say, r_{c0} from the centre, is $P^c(r_{c0}, 0) = P_{m0} - P_\infty$. The pressure distribution behind the front is taken to be uniform and equal to $P_i(0, t)$, see figure 2. It is also supposed that the pressure will redistribute itself far more quickly than the temperature, and so the latter will not have been significantly modified by the time the pressure front has formed (Zel'dovich & Raizer 1966). As the pressure transient moves outwards, dissipation will set in, and the pressure behind it drops continuously and uniformly.

Some discussion as to whether a shock wave is formed or not is appropriate here. By definition, a shock wave is a surface in a fluid through which there are sharp gradients in pressure, velocity, density, etc. Such surfaces are very thin, being of the

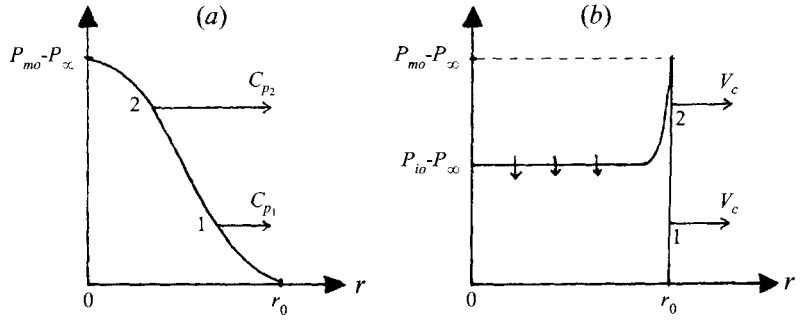

FIGURE 2. Simplified evolution of the pressure distribution in the plasma leading to shock formation: (*a*) initial Gaussian distribution with sound velocity denoted as C_p, (*b*) formed pressure front with velocity V_c; the pressure behind the front drops as the wave travels outwards. The areas under each curve should be equal.

order of a micron, and are considered surfaces of discontinuity. Effectively, the typical time of passage of a thermo-elastic pressure transient through a given point is several nanoseconds. Multiplication by the velocity of sound yields a length scale of microns (Alloncle *et al.* 1993; Vogel & Lauterborn 1988). The Tait equation of state for a liquid is assumed to hold (Cole 1948):

$$\frac{P+B}{\rho^n} = \text{const.}, \tag{4}$$

where n and B are empirical constants which depend on the nature of the liquid in question; for example, $n = 10.7$ and $B = 120$ MPa in cyclohexane. It can be shown that in the case of a maintained sharp pressure transient, the maximum condensation ratio is

$$k = \frac{\rho_0}{\rho_1} = \frac{n+1}{n-3}, \tag{5}$$

where ρ_0 and ρ_1 refer to the density in front of (undisturbed) and behind the pressure front respectively. The higher this number, the greater the likelihood of the pressure transient developing into a shock front. In the case of liquid cyclohexane, k takes a value of about 1.52. For a perfect gas, the value is 6. On this basis, it would be unwise to refer to shocks without further evidence. Recent measurements by Alloncle *et al.* (1993) of the pressure profiles and propagation velocities in the case of laser breakdown in liquids (specifically water) demonstrate that a shock wave is indeed formed, but that due to the spherical symmetry of the problem, it quickly degenerates into a pressure transient propagating at the speed of sound at a short distance from the point of breakdown. There is also experimental evidence that the velocity of the pressure transient is greater than the speed of sound very close to the energy deposition area.

The next step in this analysis is to determine the initial pressure maximum in the plasma $P_{m0} - P_\infty$, which is also assumed to be the maximum amplitude of the pressure transient/shock front at its formation, the pressure level behind the front, $P_{i0} - P_\infty$, and the maximum temperature value T_{m0}.

2.3. *The pressure amplitude and the mechanical energy* E_P

With the assumption of Gaussian distribution, the initial pressure $P_0(r)$ is given by

$$P_0(r) - P_\infty = \Delta P_0 = \frac{A}{\sigma(2\pi)^{1/2}} \exp(-r^2/\sigma^2) + A', \tag{6}$$

where A and A' are constants and σ is the standard deviation. To fix the constants suppose first that the plasma centre is the origin. Thus, the pressure will be maximum there, i.e.

$$\Delta P_{max} = P_{m0} - P_\infty = \frac{A}{\sigma(2\pi)^{1/2}} + A'. \tag{7}$$

At the edge of the plasma ($r = r_0$) the pressure $P_0(r) = P_\infty$. The expressions for A and A' are then found to be

$$A = \frac{\sigma(2\pi)^{1/2}(P_{m0} - P_\infty)}{1 - \exp(r_0^2/2\sigma^2)}, \quad A' = \frac{-(P_{m0} - P_\infty)\exp(-r_0^2/2\sigma^2)}{1 - \exp(-r_0^2/2\sigma^2)} \tag{8}$$

which when substituted into (6) gives

$$P_0(r) - P_\infty = \frac{P_{m0} - P_\infty}{1 - \exp(r_0^2/2\sigma^2)}[\exp(-r^2/2\sigma^2) - \exp(-r_0^2/2\sigma^2)]. \tag{9}$$

The 'equivalent' mechanical energy, E_P, injected into the liquid is related to the pressure via the expression

$$E_P = \iiint_V \Delta P \, \mathrm{d}V = \int_0^{r_0} (P(r) - P_\infty) 4\pi r^2 \, \mathrm{d}r. \tag{10}$$

The energy injection is taken to occur instantaneously at time $t = 0$. For $t > 0$, there is no other source of energy appearing and thus the above integral is valid at all times if dissipation is assumed negligible. Therefore it is possible to use the initial pressure distribution $P_0(r)$ (expression (9)) in (10), giving

$$E_P = 4\pi \int_0^{r_0} \frac{(P_{m0} - P_\infty)}{1 - \exp(-r_0^2/2\sigma^2)}[\exp(-r^2/2\sigma^2) - \exp(-r_0^2/2\sigma^2)] r^2 \, \mathrm{d}r. \tag{11}$$

The first expression on the right-hand side is integrated using the substitution-of-variables method ($Y = r^2/2\sigma^2$), giving an incomplete Gamma function and (11) thus becomes

$$E_P = \frac{4\pi}{3} \frac{P_{m0} - P_\infty}{1 - \exp(-r_0^2/2\sigma^2)}[3\sigma^3(\tfrac{1}{2}\pi)^{1/2} \Psi(\tfrac{3}{2}, r_0^2/2\sigma^2) - r_0^3 \exp(-r_0^2/2\sigma^2)]. \tag{12}$$

The pressure difference $P_{m0} - P_\infty$ is then written

$$P_{m0} - P_\infty = \frac{3}{4\pi} E_P \frac{1 - \exp(-r_0^2/2\sigma^2)}{3(\tfrac{1}{2}\pi)^{1/2} \sigma^3 \Psi(\tfrac{3}{2}, r_0^2/2\sigma^2) - r_0^3 \exp(-r_0^2/2\sigma^2)}. \tag{13}$$

As the pressure transient travels outwards, the pressure behind it is taken to be uniform and equal to the value at the centre $r = 0$. Thus, from (10), with $P(r) = P(0) = P_{i0} =$ constant, one obtains

$$P_{m0} - P_\infty(r = 0) = P_{i0} - P_\infty = \frac{3}{4\pi} \frac{E_p}{r_0^3}, \tag{14}$$

i.e. only the uniform pressure behind the transient is taken into account, the contribution to the integral from the thin transients themselves being negligible. Expression (14) relates the maximum pressure amplitude in the shock wave to the proportion of injected energy transformed into mechanical energy. The important unknown here is the total mechanical energy E_P, which must now be evaluated by physically examining how it is divided up between the pressure wave and the bubble.

2.4. *Mechanical energy distribution in the plasma*

It was assumed that the mechanical energy E_P is a percentage (10–20) of the total injected energy W_i and that it is further divided into that taken by the pressure transient (or shock wave) E_{sw} and that of the bubble itself E_b, i.e.

$$E_P = E_{sw} + E_b. \tag{15}$$

2.4.1. *The energy corresponding to the pressure transient/shock wave*

Initially, the energy of the pressure transient and of the bubble mainly correspond to impulse motion (Hentschel & Lauterborn 1982). These authors showed that the pressure wave energy is given by the impulse expression (Cole 1948)

$$E_{sw} = \frac{4\pi r_{c0}^2}{\rho_\infty C_\infty} \int_0^\infty (P(t) - P_\infty)^2 \, \mathrm{d}t = \tfrac{1}{2}\theta(r_{c0}) \frac{4\pi r_{c0}^2}{\rho_\infty C_\infty} (P_{m0} - P_\infty)^2 = \frac{8\pi r_{c0}^3 (P_{m0} - P_\infty)^2}{\rho_\infty C_\infty^2}, \tag{16}$$

where $\theta(r_{c0}) \approx 4r_{c0}/C_\infty$ is the shock wave time constant (Brinkley & Kirkwood 1947). Here C_∞ is the speed of sound in the liquid at (P_∞, T_∞) and ρ_∞ is the liquid density under the same conditions. (It is also obtained by squaring the shock wave velocity, given by the Hugoniot–Rankine relation, and multiplying by liquid density and volume.)

Combining equations (15), (16) and (13) gives a quadratic equation in $P_{m0} - P_\infty$, for which the solution is

$$P_{m0} - P_\infty = \tfrac{1}{2}(b + \Delta^{1/2}), \tag{17}$$

where $\Delta = b^2 - 4c$ and

$$b = \frac{\rho_\infty C_\infty^2}{6r_{c0}^3} \frac{3(\frac{1}{2}\pi)^{1/2}\sigma^3 \Psi(\frac{3}{2}, r_0^2/2\sigma^2) - r_0^3 \exp(-r_0^2/2\sigma^2)}{1 - \exp(-r_0^2/2\sigma^2)}, \quad c = \frac{\rho_\infty C_\infty^2}{8\pi r_{c0}^3} E_b.$$

Obviously, Δ must be $\geqslant 0$. E_b and σ are, theoretically, the only unknowns in the above expression for $P_{m0} - P_\infty$, and thus, for a given value of E_b, a minimum limiting value for σ can be defined: $\sigma_{lim} = f(E_b, r_0)$. On closer examination of the above expressions, this should more properly be written $\sigma_{lim} = f(E_b, r_0, \rho_\infty, C_\infty)$. In bubble generation by localized deposit of energy, it has been well verified that the energy of the bubble is directly proportional to the injected energy (Giovanneschi-Testud 1987; Kattan 1990). Further, in this case of the electrical formation of a bubble following a current impulse, the plasma radius is close in value to the radius of curvature of the point electrode. The equivalent physical dimension in laser-induced breakdown could be chosen to be the radius of the focal spot. Applying the Vashy–Buckingham theorem to the function $\sigma_{lim} = f(W_i, r_p, \rho_\infty, C_\infty)$ leads to the existence of a direct relationship between the following two non-dimensional numbers: σ_{lim}/r_p and $W_i/(r_p^3 \rho_\infty C_\infty^2)$. Using the Tait equation on the second of these changes it to $W_i/(r_p^3 nB)$. Though there is no obvious means to fix the relationship between these, the most simple mathematical relationship is that of proportionality. This clearly has no *a priori* physical basis, it merely allows a first-order estimate for σ_{lim}, since exact values can be ascribed to W_i, r_p, n and B. Supposing the constant to be 1 (it would be of order 1) gives the following values for σ_{lim} in cyclohexane, n-decane and n-pentane respectively: 69, 44 and 41 %.

It is possible to give reasonably accurate experimental values to E_b and guess the value of σ bearing the above calculation in mind, assuming that its influence is not too dramatic. Typical values are given in table 1 for a number of different liquids for $P_{m0} - P_\infty$ and E_{sw} (% of W_i) as a function of energy injection, radius of curvature of the point and the applied hydrostatic pressure.

	cyclohexane	n-decane	n-pentane	water
W_i (nJ)	2.00	0.35	0.37	1800.00
r_0 (μm) $\approx r_p$	1.50	0.70	1.10	140
P_∞ (MPa)	1.00	1.00	1.00	0.10
P_c (MPa)	4.07	2.12	3.37	2.21
T_c (K)	553.50	617.70	469.70	647.30
E_b (% of W_i)	2.00	1.90	1.30	2.90
n	10.70	10.00	13.30	7.15
B (MPa)	121.80	115.10	45.50	300.00
σ (% of r_0)	75	95	55	100
r_c (μm)	6.20	3.30	5.50	593.40
P_{g0} (MPa)	15.70	14.90	5.87	22.70
$P_{m0}-P_\infty$ (MPa)	61.29	57.99	23.41	113.30
$T_{m0}-T_\infty$ (K)	1223.60	1754.20	1206.50	921.00
E_{sw} (% of W_i)	12.13	10.66	8.18	23.06
E_{in} (% of W_i)	55.29	64.28	62.09	32.22
E_v (% of W_i)	30.58	23.16	27.93	41.82
E_P (% of W_i)	14.13	12.56	9.48	25.96
E_T (% of W_i)	85.87	87.44	90.02	74.04

TABLE 1. Physical constants, given and derived theoretical values of a number of quantities in cyclohexane, n-decane and n-pentane in the case of electrically generated bubbles and in water for a laser-generated bubble.

Clearly, pressures inside the plasma can be very high (> 50 MPa). In the case of laser breakdown in water, Alloncle *et al.* (1993) extrapolate to initial values of the order of 10^2 MPa from their experimental results.

Finally, from (17), it can be seen that the pressure $(P_{m0}-P_\infty)$ is related to the square-root of the bubble energy E_b. It is known that the bubble energy is proportional to the injected energy W_i (Giovanneschi-Testud 1987, and figure 9 here), giving a direct relationship between $(P_{m0}-P_\infty)$ and $(W_i)^{1/2}$. In fact, using typical order-of-magnitude values in (17) for this type of problem yields that $(P_{m0}-P_\infty)$ is almost directly proportional to $(W_i)^{1/2}$. Recently, in laser-induced breakdown, Noack & Vogel (1995) obtained the experimental result $(P_{m0}-P_\infty) \propto (W_i)^\beta$, with $\beta = 0.52$. Though it requires further experimental investigation, it is, nevertheless, possible to say that expression (17) and its derivation do have some experimental backup, albeit scant at present.

2.5. *Thermal energy within the plasma*

The maximum temperature T_{m0} due to the energy injection is estimated as follows. Experimental evidence shows that the deposition of charge into the liquid does not occur instantaneously: there is a necessary absorption time t_{abs}. In cyclohexane, this is of the order of 10^{-12} s. The temperature distribution $g(r)$ is assumed to remain Gaussian during this time. The energy thus absorbed is internal (E_{in}). The remaining thermal energy is stocked as latent heat of vaporization L_v such that $E_v = NL_v$ where N is the number of vaporized molecules. Clearly the liquid will have a very high thermal resistance compared to the gas/vapour (Nigmatulin, Khabeev & Nagiev 1981) and thus N will be given by (Kattan *et al.* 1989)

$$N = \tfrac{4}{3}\pi \frac{P_\infty R_m^3}{r_g T_b}, \tag{18}$$

where r_g is related to the perfect gas constant and given by $r_g = 8.314$ J K^{-1} and R_m is the maximum radius of the bubble.

The expression for the internal energy is given by Hu (1969):

$$d^2E_{in} = C_v \rho_c 4\pi r^2 dr \left[\frac{\partial \theta}{\partial \tau} d\tau\right], \tag{19}$$

where C_v is the calorific capacity at constant volume and ρ_c is the critical density of the liquid. The function θ is given by

$$\theta(r, t) = T(r, t) - T_\infty = (T_{m0} - T_\infty)\, g(r) f(\tau), \tag{20}$$

where $f(\tau) = f(t/t_{abs})$ is a function going from 0 to 1 during the absorption time and

$$g(r) = \frac{1}{1 - \exp(-r_0^2/2\sigma^2)} [\exp(-r^2/2\sigma^2) - \exp(-r_0^2/2\sigma^2)]. \tag{21}$$

Any diffusion of heat by conduction is justifiably neglected in the time scale involved. The hypothesis is also made that

$$\int_0^1 f'(\tau)\, d\tau = 1. \tag{22}$$

This implies that the absorption of energy is complete and takes place in a time shorter than that necessary for the pressure transient to form. This is verified in most of the liquids studied experimentally, the notable difference being for liquid argon (Hernandez-Avila *et al.* 1994). It is not possible to say at present whether this will be the case for all cryogenic liquids (McCluskey & Denat 1996). Therefore, for the liquids considered, the temperature reaches its maximum value when $f(\tau) = 1$, and due to the rapidity of the process it can be said that the temperature rise is almost instantaneous. Furthermore, C_v is assumed to be constant. This is obviously not the case physically: it is a simplification made in the model.

Integrating (19) with respect to τ and using hypothesis (22) gives

$$dE_{in} = C_v \rho_c 4\pi r^2 g(r)\, dr (T_{m0} - T_\infty). \tag{23}$$

Integrating a second time with respect to the radius up to $r = r_0$ and combining the result with (11) leads to an expression for the maximum temperature at the centre of the plasma:

$$T_{m0} - T_\infty = \frac{E_T - E_v}{E_P} \frac{\gamma - 1}{\rho_c R_g} (P_{m0} - P_\infty). \tag{24}$$

R_g is the perfect gas constant (287 J kg^{-1} K^{-1}) and γ the ratio of calorific capacities. Some computed values for two experimental liquids are given in table 1. The energy ratio in (24), $(E_T - E_v)/E_P$, has this form since the temperature rise is due to the increase in internal energy only: phase change takes place at constant temperature.

It is clear from this that the plasma temperature, though above the critical temperature is still 'low'. It is in this sense that the plasma may be termed cold.

The model presented here to account for the internal energy is an improvement on that of Kattan *et al.* (1989). That particular model breaks down when the applied pressure goes above the critical value P_c. That is, the liquid in the plasma zone heats to the boiling temperature and then changes phase. The initial temperature of the vapour is the boiling temperature, which is only defined as long as $T_b < T_c$. By introducing the internal energy in the form of (19), this is no longer a problem since the vapour temperature after phase change can continue to rise above the boiling temperature.

In expressions (17) for the pressure and (24) for the temperature, the outstanding unknown in the system is E_b, the energy of the bubble. Its derivation is now necessary.

2.6. *The energy of the bubble*

The outward radial velocity of the liquid given by Rayleigh (1917) is $u = r_0^2 r_0'/r^2$, where r_0 is taken to be the initial radius of the bubble when formed. Note that r_0 is also the radius of the plasma volume. The prime denotes differentiation with respect to time. The bubble energy is simply kinetic energy, i.e. viscosity is considered negligible (Watson, Chadband & Sadeghzadeh-Araghi 1991), and therefore

$$E_b = \tfrac{1}{2}\rho_c \int_{r_0}^{\infty} 4\pi r^2 u^2 \, \mathrm{d}r = \rho_c 2\pi \left(\frac{\mathrm{d}r_0}{\mathrm{d}t}\right)^2 r_0^3. \tag{25}$$

The (as yet) unknown interfacial velocity $\mathrm{d}r_0/\mathrm{d}t$ is linked to the pressure difference across the interface. The initial pressure distribution is such that the first pressure transient (the shock wave) has to be emitted in the liquid phase since an interface has not formed. A stable interface is formed only when the resulting pressure drop is enough to bring the absolute pressure to below the critical value. (It is necessary to make this somewhat arbitrary definition of the bubble interface in order to be able to determine the moment after which it is possible to refer to a bubble rather than a zone of indeterminate phase.) The spherical interface will then (instantaneously) form around a volume of vapour. Since, as yet, no change of volume has occurred, the pressure of the high-temperature vapour within the interface (or bubble) will be much greater than the pressure outside. As a consequence of this 'trapped' pressure difference across the interface the bubble will expand radially. Thus the velocity of the bubble interface, by analogy with the Hugoniot–Rankine relation will be of the form

$$\frac{\mathrm{d}}{\mathrm{d}t} r_0 = \frac{P_{g0} - P_\infty}{\frac{1}{2}\rho_c C_\infty} = U_0. \tag{26}$$

Here P_{g0} is the initial gas pressure inside the bubble and ρ_c is an intermediate density value since neither ρ_l (liquid density) nor ρ_g (gas density) are relevant to the interface itself in these circumstances. Since the time scale for condensation is too long compared to the dynamic scales involved here, it is not unreasonable to suppose that ρ_c takes a value close to the critical density value corresponding to the critical pressure and volume of the liquid in question The numerator in (26) is simply the pressure difference across the interface. Thus the bubble energy is given by

$$E_b = 8\pi r_0^3 \frac{(P_{g0} - P_\infty)^2}{\rho_c C_\infty^2}. \tag{27a}$$

In terms of the pressure difference, this is

$$P_{g0} - P_\infty = C_\infty \left(\frac{\rho_c}{8\pi} \frac{E_b}{r_0^3}\right)^{1/2}. \tag{27b}$$

Clearly, this pressure difference can only be evaluated when the percentage of energy transferred to the bubble is known. Thus, once E_b and σ are known it is then possible to evaluate the pressure $P_{m0} - P_\infty$ from (17) and $P_{g0} - P_\infty$ from (27*b*).

It is now possible to estimate the bubble lifetime and size if, in conjunction with equation (28*b*), adiabatic expansion for the bubble is assumed (Prosperetti 1991) along with the approximate condition that at $r = R_m$ the pressure $P = P_\infty$. Although bubble expansion is not adiabatic over the entire cycle of growth and collapse, the

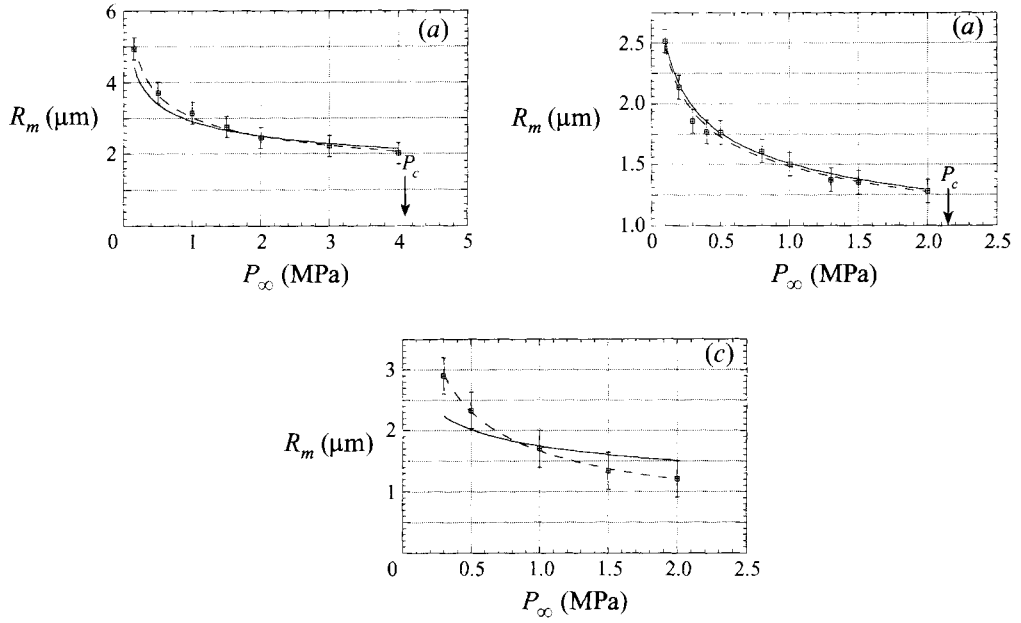

FIGURE 3. Comparison between the theoretical curve for R_m as a function of P_∞ (solid line) and published experimental results (symbols with error bars). The dashed line is the best fit of the experimental results and is only included as a visual aid. (*a*) Cyclohexane with $W_i \approx 2$ nJ, $r_p = 1.5$ μm (Kattan *et al.* 1991), (*b*) n-decane with $W_i \approx 0.35$ nJ, $r_p = 0.7$ μm (Kattan 1990) and (*c*) n-pentane with $W_i \approx 0.37$ nJ, $r_p = 1.1$ μm (Kattan 1990).

approximation does not introduce too great an error when calculating the maximum bubble radius. The relevant equations for adiabatic bubble expansion are

$$R_m \approx r_0(P_{g0}/P_\infty)^{1/3\gamma} \tag{28a}$$

and

$$t_r \approx 1.83\, R_m(\rho_\infty/P_\infty)^{1/2}. \tag{28b}$$

The curves shown in figures 3(*a*), 3(*b*) and 3(*c*) are for the liquids cyclohexane, n-decane and n-pentane, for which data are available. They will be discussed later.

3. Bubble formation due to breakdown of the liquid

This section is an examination of the effects of the outgoing pressure wave on the (non-equilibrium) plasma and on the initial growth of the bubble.

3.1. *Behind the pressure transient/shock front*

Once the shock front is formed, it moves through the liquid, compressing it. The pressure at a radial position r in the liquid passes from P_∞ to P_1 such that

$$\frac{P_1+B}{P_\infty+B} = 1+\frac{2n}{n+1}(M_c^2-1), \tag{29}$$

where M_c is the Mach number of the shock front. Equation (29) is derived from combining the equations of conservation of mass and momentum across the shock wave with the Tait equation of state for a liquid. It is analogous to the expression for shock waves in a perfect gas, where $B = 0$ and the coefficient of the term in parenthesis is γ. Generally, in this geometry the amplitude of a propagating wave decreases as $1/r$

(Cole 1948). For the amplitude of the pressure transient, Brinkley & Kirkwood (1947) obtained the following expression (the acoustic approximation):

$$P(r_c, t) - P_\infty = \frac{r_{c0}}{r_c(t)}(P_{m0} - P_\infty), \tag{30}$$

where $r_c(t)$ denotes the position of the pressure transient at time t and $r_c \geqslant r_{c0}$.

Rather than using the Langrangian form of the equations it is more instructive to proceed in an Eulerian frame of reference (see, for example, Church 1989). At a fixed position r_c, Church assumed that the pressure variation there was similar to the response of an RC circuit, i.e.

$$P(t) - P_\infty = \frac{r_{c0}}{r_c(t_c)}(P_{mo} - P_\infty)\exp(-(t-t_c)/\theta(r_c)), \tag{31}$$

where t_c is the time taken by the shock front to reach the position r_c and $\theta(r_c)$ is the time constant of the shock wave. From (31) it is clear that, at r_c, the liquid becomes less and less compressed in time with the passage of the shock wave. In other words, $P(r_c, t+\Delta t) < P(r_c, t)$. The pressure behind the shock is quasi-uniform and some mechanism needs to be envisaged to bring about intermediary pressure values between $P(r_c, t+\Delta t)$ and $P(r_c, t)$, in order to explain why the shock profile is not discontinuous behind the maximum amplitude as it is in front of it. To this end, the shock wave is considered to be a source of pressure waves (i.e. an acoustic source) and therefore the acoustic approximation can be used for the liquid behind it. It is now possible to estimate the effect of this acoustic source on the spherical volume $r < r_c$. The equations of continuity and momentum in spherical polar coordinates are then written, respectively,

$$\frac{\partial u}{\partial t} = -\frac{1}{\rho_\infty}\frac{\partial P}{\partial r} \tag{32}$$

and

$$\frac{1}{C_\infty^2}\frac{\partial P}{\partial t} = -\rho_\infty \frac{1}{r^2}\frac{\partial}{\partial r}(r^2 u) \tag{33}$$

for $0 \leqslant r \leqslant r_c$ (u is the radial velocity of the liquid). If (33) is differentiated with respect to t, and the liquid velocity eliminated using (32), the following solution to the system is obtained (using (31)):

$$P(r, t) - P_\infty = \frac{r_c - r_{c0}}{r - r_c}\left[\frac{r_0}{r_c}(P_{m0} - P_\infty)\exp(-(t-t_c)/\theta(r_c)) + O(1/C_\infty)\right]. \tag{34}$$

In terms of the velocity the solution is

$$u(r, t) - u(r, t_0) = -\frac{P(r, t) - P_\infty}{\rho_\infty C_\infty} + \frac{P(r, t_0) - P_\infty}{\rho_\infty C_\infty} + \frac{1}{\rho_\infty}\frac{1}{r - r_{c0}}\int_{t_0}^{t}(P(r, t') - P_\infty)\,\mathrm{d}t'. \tag{35}$$

It is of some significance to examine these two solutions in detail. For $0 \leqslant r < r_0$, the factor $(r_c - r_{c0})/(r - r_c)$ in (34) is strictly negative, since $r_{c0} < r_c$. Therefore, $(P(r, t) - P_\infty) < 0$. It is not difficult to deduce from this that the right-hand side of (35) is positive, i.e. that $(u(r, t) - u(r, t_0)) > 0$. (Note that the second term in (35) is positive since $P(r, t_0) = P_{i0} > P_\infty$.) This means that the liquid is entrained by, and accelerates outwards behind, the pressure transient. The liquid thus stressed (radially outward flow from a point) will cavitate and a bubble will form. This is clearly a more rigorous formulation of the 'afterflow' effect discussed by Cole (1948) and goes towards giving theoretical justification to some of the experimental results of McCluskey & Denat (1996). An outgoing spherical pressure transient will cause the pressure behind it to

drop and bring about circumstances where a bubble interface can form. The relative positions of both the pressure transient and the bubble at that instant are calculated in the next subsection.

3.2. *Position of pressure transient at liquid breakdown*

For this a relationship between the radial distance r_c and the initial known quantities is needed. The amplitude and velocity of spherical wave motions decrease as the wave travels outwards. Thus, a shock front with velocity V_c will eventually slow to the velocity of sound C_∞. Cole (1948), via the theory of Kirkwood & Bethe (1942), gives an expression for the velocity of the shock front:

$$M_c = \frac{V_c}{C_\infty} = 1 + \frac{n+1}{4C_\infty} u, \tag{36}$$

where, from Hugoniot's relation,

$$u = \frac{P_{m0} - P_\infty}{\rho_\infty V_c} \frac{r_{c0}}{r_c}$$

(i.e. the acoustic approximation, since $u \to 0$ when $r_c \to \infty$ and $V_c \to C_\infty$. Using this in (36) gives

$$M_c^2 - M_c - \tfrac{1}{4}(n+1) \frac{r_{c0}}{r_c} \frac{P_{m0} - P_\infty}{\rho_\infty C_\infty^2} = 0 \tag{37}$$

which has the solution

$$M_c = \tfrac{1}{2} + \tfrac{1}{2} \left[1 + (n+1) \frac{r_{c0}}{r_c} \frac{P_{m0} - P_\infty}{\rho_\infty C_\infty^2} \right]^{1/2}. \tag{38}$$

The Mach number is eliminated from (38) by substituting it into (29) and expanding. To first approximation, one obtains

$$\frac{P_1 + B}{P_\infty + B} = 1 + n \frac{r_{c0}}{r_c} \frac{P_{m0} - P_\infty}{\rho_\infty C_\infty^2}. \tag{39}$$

If the pressure in the bubble when it is formed is P_{g0}, then the pressure in the liquid behind the shock wave is related to P_{g0} via the momentum balance normal to the interface:

$$P_1 = P_{g0} - 2\sigma / r_0 \approx P_{g0}. \tag{40}$$

The simplifying assumption that $r_{c0} = r_0$ is made and from this it can be deduced that the radial position of the pressure transient at the instant of the bubble formation is

$$r_c = n r_0 \frac{P_{m0} - P_\infty}{P_{g0} - P_\infty} \frac{P_{m0} + B}{\rho_\infty C_\infty^2}. \tag{41}$$

Typical calculated values are given in table 1.

The value of approximately 600 μm for r_c in the water case corresponds to a time of the order of 300 ns (Giovanneschi-Testud 1987), which is close to the experimental delay between the luminous flash of the initial plasma and the appearance of the bubble (Alloncle *et al.* 1993).

4. Results and discussion

The curves of the maximum bubble radius as a function of applied pressure are given in figures 3(*a*), 3(*b*) and 3(*c*). The corresponding experimental results are also shown. The remarkable agreement indicates that the series of approximations made in the

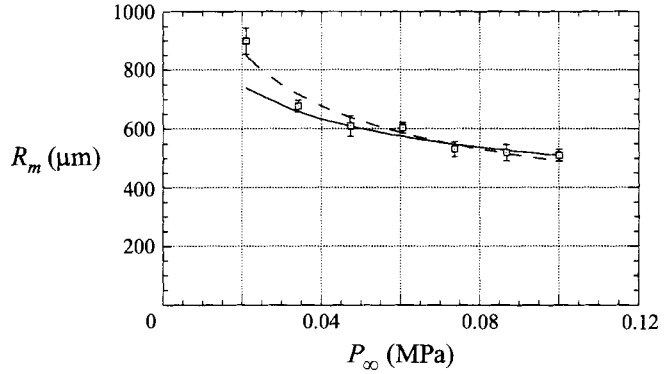

FIGURE 4. Comparison between the theoretical curve (solid line) for R_m as a function of P_∞ and experimental results (symbols with error bars) of laser breakdown in water (Giovanneschi-Testud 1987). $W_i \approx 1.8$ mJ. The dashed line is the best fit of the experimental results.

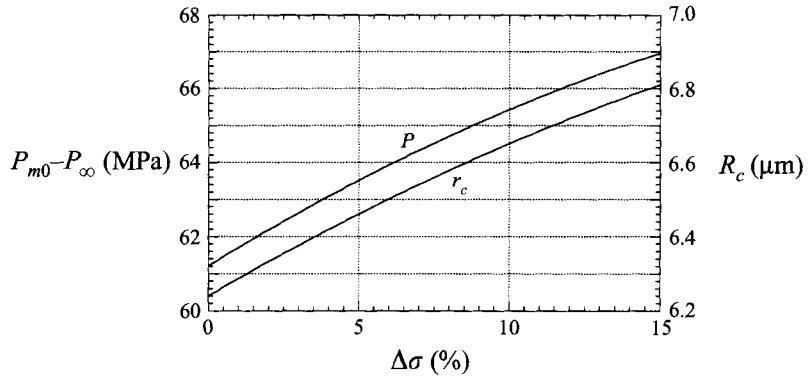

FIGURE 5. Sensitivity of the initial maximum pressure in the plasma $P_{m0}-P_\infty$ and of the initial radius of the plasma $r_c(\approx r_0)$ to errors in the value of the standard deviation σ of the Gaussian distribution curve (equation (1)) for cyclohexane. The variation in both is less than 10% for an error of 15% in σ.

above analysis does not violate the energy conservation laws, and one can expect to closely predict the maximum sizes of bubbles in these liquids given only the injected energy W_i and the value of E_b. Agreement, however, for n-pentane was less good, though the experimental results did not follow a $(W_i/P_\infty)^{1/3}$ law. In each case, bubbles were detected up to pressures close to the critical value. In the case of optical breakdown in water (figure 4) there is a very close correspondence between theory and experiment over all but the lowest values of the applied pressure. This is because the lowest pressures approach the vapour pressure for water, and other phenomena may be expected to intervene.

There are a number of parameters appearing in the above analysis for which values were chosen, i.e. σ, the standard deviation in the Gaussian distributions of equation (1), and r_0, the initial size of the plasma and the bubble. Figure 5 shows the sensitivity of both r_c and $P_{m0}-P_\infty$ in cyclohexane when σ is varied by 15% around its chosen value, i.e. that calculated using (17). In both cases, the variation is less than 10%, which implies that an error in the choice of σ does not have a significant effect on the rest of the calculated quantities. This is important since it is not possible to verify experimentally the initial distribution of energy in the plasma.

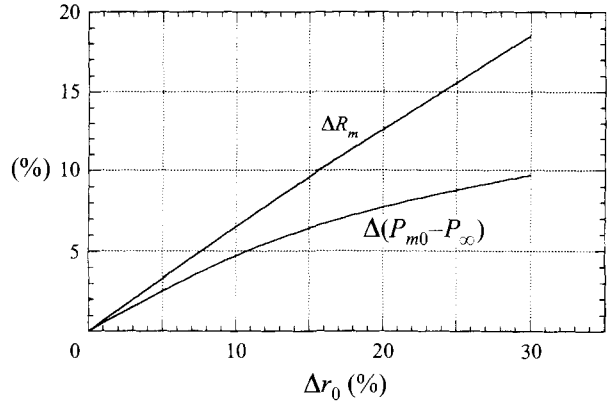

FIGURE 6. Sensitivity of the initial maximum pressure in the plasma $P_{m0}-P_\infty$ and of the maximum bubble radius R_m to errors in the value of the plasma radius r_0, for cyclohexane. Though the pressure is relatively insensitive to changes in the value of r_0, the opposite is the case for R_m. This could be the cause of any divergence between theory and experiment.

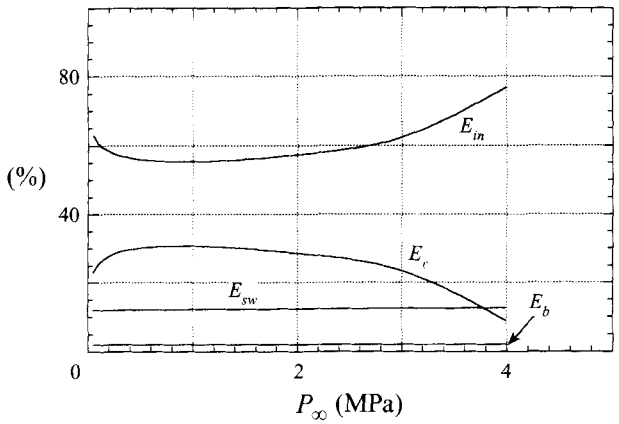

FIGURE 7. The balance between the different components (mechanical (E_b+E_{sw}) and thermal $(E_{in}+E_v)$) of the total injected energy $W_i(=E_b+E_{sw}+E_{in}+E_v)$ as a function of the applied hydrostatic pressure P_∞ in cyclohexane. See §§2.4 and 2.5 in the text for the definitions of each term. The thermal energies account for approximately 85% of the total. Curves for other liquids are expected to be similar.

Figure 6 shows how the maximum bubble radius and the initial pressure difference are affected by varying the value of r_0, again in cyclohexane. A 30% change in its value causes the pressure to vary by only 10%. The maximum bubble size is, however, quite sensitive to this quantity, and it is therefore possible that divergence between theory and experimental values could be attributable to an erroneous choice of r_0. The agreement between the theory and the experimental results, however, serves as a justification for the choice of values for these parameters. Experimental evidence suggests that it is unlikely that a large error in the value of r_0 would be made.

The energy balance is given on figure 7. The internal energy is the main component throughout, as is to be expected. The distribution of the thermal energy is, however, different to what would be initially expected. As E_v is defined as NL_v, it is reasonable to assume that E_v will vary as L_v. This happens for the higher values of the pressure. At low values, it unexpectedly drops, even though it is known that as the pressure

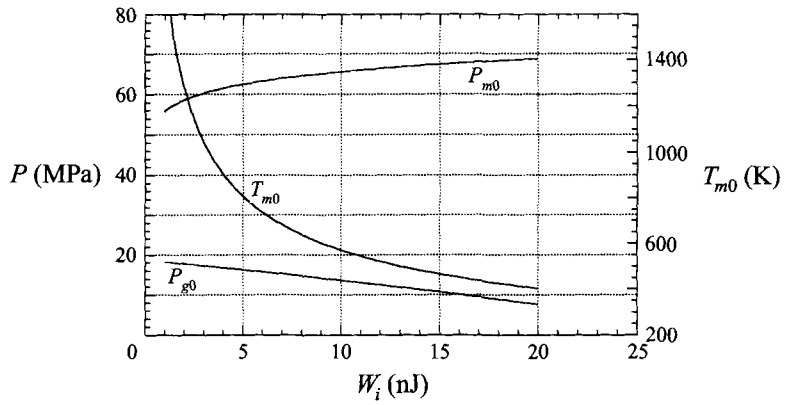

FIGURE 8. Evolution of the initial pressure maximum $P_{m0}-P_\infty$ and the initial temperature maximum T_{m0} in the plasma, and the initial pressure of the vapour in the bubble when formed, P_{g0}, as a function of the injected energy W_i for the liquid cyclohexane. The necessary experimental data linking r_0 to W_i are taken from Kattan (1990). The maximum temperature in the plasma drops dramatically as injected energy is increased, since the plasma zone volume will necessarily be substantially bigger. Its dimensions depend on the radius of curvature of the point.

drops, L_v increases. Clearly, it is the variation of N, the number of molecules changed into vapour, which begins to dominate. Fewer molecules of liquid are vaporized below a certain pressure due to the high value of L_v. The maximum bubble radius R_m increases as the pressure decreases, as is seen from experiments, and from (18), the pressure and corresponding boiling temperature variations are stronger than the bubble size variation and so N drops.

The total mechanical energy is always of the order of 15%.

Figure 8 presents the evolution of the maxima of initial temperatures and pressures in the plasma, T_{m0} and $P_{m0}-P_\infty$ respectively, and the initial pressure of the vapour in the bubble when formed, P_{g0}, as functions of the injected energy W_i. Some experimental data are needed as input in this calculation: $r_0 \approx r_p$ and the relationship linking r_p and W_i (Kattan 1990). It is seen that the initial pressure at the plasma centre increases as the injected energy increases, whereas the temperature drops rather dramatically. This is explained by the fact that in order to get higher injection levels the point tip r_p is necessarily larger. Typically the plasma zone has the same dimensions as r_p, i.e. $r_0 \approx r_p$, and is thus correspondingly bigger. A much greater volume of liquid needs to be heated with the result that the maximum temperature is lower. There will therefore be an upper limit to this process, when the avalanche/plasma zone is too spread out. Other processes, such as the total energy deposition time, will probably alter substantially in these cases, causing the above analysis to be inapplicable. It may be possible to explain the observed phenomena in a cryogenic liquid, argon, along these lines (McCluskey & Denat 1996).

The pressure variation fits with experimental evidence in that the detected shock waves have greater amplitudes as W_i increases.

The breakup of energy in real terms (figure 9) shows that the amount of mechanical energy taken by the shock wave increases at a faster rate than that of the thermal processes as the energy level increases and eventually assumes a similar magnitude. At the low energy injection values, the most important component becomes the internal energy (E_T-E_v). This is consistent with the physics of the problem, since before any phase change can take place, the liquid must be heated.

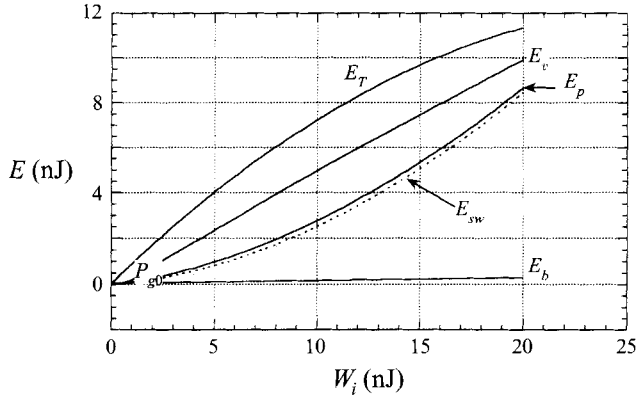

FIGURE 9. Evolution of the thermal, $E_T(= E_v + E_{in})$, and mechanical, $E_P(= E_b + E_{sw})$, energies as a function of injected energy in cyclohexane. At low injected energy values, the internal energy is the most important component. The necessary experimental data are taken from Kattan (1990).

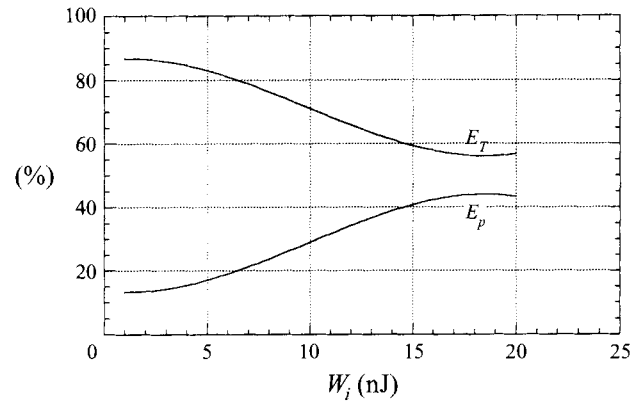

FIGURE 10. Evolution of thermal and mechanical energies (as percentages of the total injected energy W_i) plotted as a function of the total injected energy in cyclohexane. Although the relative amount of energy taken by the mechanical processes increases over most of the range of W_i, there is never a point at which they take more energy than the thermal processes. The data are taken from figure 9.

In terms of percentages of W_i, the mechanical processes increase in relative importance compared to the thermal ones, both levelling off at higher energies (figure 10).

The final curve (figure 11) shows the position of the pressure transient/shock wave at the moment when the bubble is properly formed. Our assumption that bubble growth is influenced by being formed in the decreasing tail of the outgoing pressure wave appears quite feasible for smaller bubbles (low W_i). Its relative position at the higher values of W_i indicates that its influence is limited to a smaller proportion of the bubble growth period.

It is reasonable to conclude at this stage that the series of assumptions made on the physical processes taking place following a rapid localized deposition of energy into a fluid are correct, as are the conclusions of the analysis for both methods of artificial bubble generation (laser and electrical). These are now listed.

(i) Following a large enough energy deposition, the temperature and pressure of the

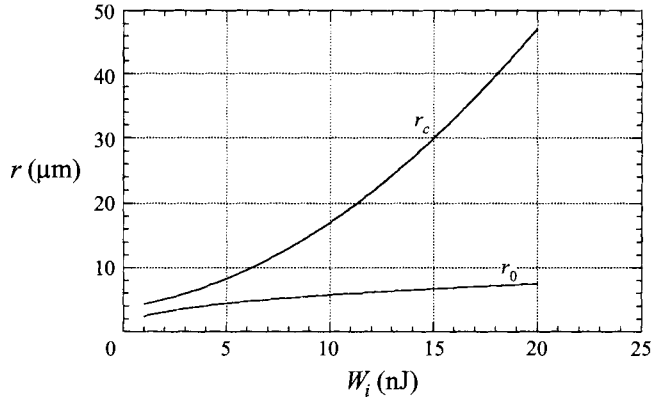

FIGURE 11. Position of the outgoing pressure transient r_c relative to the initial bubble radius r_0 plotted as a function of the injected energy W_i. This is indicative of the relative velocities of the bubble interface and the pressure transient. For low energy injections ($W_i < 5$ nJ), the pressure transient has not travelled far enough away from the bubble to avoid influencing its behaviour. For larger bubbles/energy deposits the shock wave travels further faster, thus decreasing its influence on the bubble growth.

liquid rise to values well above the critical values, and a non-equilibrium plasma forms. The distributions of both pressure and temperature are Gaussian within the plasma and uniform and unchanged outside.

(ii) The energy divides into two components: about 85% to thermal effects and 15% to mechanical.

(iii) The pressure redistributes itself more quickly than the temperature: a pressure transient is emitted, accompanied by a drop in pressure in the centre of the plasma region. When this goes below the critical level, a bubble interface forms, of dimensions close to those of the plasma, behind the outgoing pressure wave/shock wave.

(iv) Once the pressure at the centre has dropped, the temperature of the liquid will be high enough to vaporize it. The bubble grows rapidly due to the expansions of the (pressurized) vapour. It reaches a maximum size when the internal vapour pressure falls below the ambient hydrostatic pressure and collapses in on itself.

(v) At the same time, the outgoing pressure transient induces an outward radial flow of the liquid behind it. This is the 'afterflow' referred to by Cole (1948). The spherical geometry means that a flow singularity occurs since there is no source of matter. Such an effect is masked due to the simultaneous vaporization of the liquid and expansion of the compressed vapour.

(vi) The initial pressures and temperatures are calculated and found to be well above the critical values. The computed values seem reasonable: 10^3 K for $T_{m0}-T_\infty$, 50 MPa for $P_{m0}-P_\infty$ and 15 MPa for the initial pressure of the vapour within the bubble P_{g0}.

(vii) The supposition that the bubble expansion is adiabatic does not lead to serious discrepancy with experimental results. This is to be expected when only considering the first cycle of bubble growth.

The model presented in this paper provides a formal link between the initial energy injection into the liquid and the formation of a pressure transient and a vapour bubble. It will be of great importance when treating the subsequent dynamical motion of the bubble and the influence on it by the outgoing pressure transient.

The authors would like to express their thanks to Dr Anne-Patricia Alloncle of the

Institute of Fluid Mechanics, Marseille, for her invaluable comments during the course of this work.

REFERENCES

ALLONCLE, A. P., DUFRESNE, D. & AUTRIC, M. 1993 Characterisation of pressure waves in liquids using an interferometric method. *IUTAM Symp. on Bubble Dynamics and Interface Phenomena, Birmingham, UK.*

ALLONCLE, A. P., VIERNES, J., DUFRESNE, D., CLEMENT, X., GUERIN, J. M. & TESTUD, P. 1990 Study of the interaction of a high power laser radiation and a transparent liquid. *8th Intl. Symp. on Gas Flow and Chemical Lasers, Madrid, Spain, SPIE* 1397, pp. 675–678.

BESANT, W. 1859 *Hydrostatics and Hydrodynamics.* Deighton Bell, Cambridge.

BRINKLEY JR., S. R. & KIRKWOOD, J. G. 1947 Theory of the propagation of shock waves. *Phys. Rev.* **71**, 606–611.

CHURCH, C. C. 1989 A theoretical study of cavitation generated by an extra-corporeal shock wave lithotripter. *J. Acoust. Soc. Am.* **86**, 215–227.

COLE, R. H. 1948 *Underwater Explosions.* Princeton University Press.

COLEMAN, A. J. & SAUNDERS, J. E. 1989 A survey of the acoustic output of commercial extracorporeal shock wave lithotripers. *Ultrasound Med. Biol.* **15**, 213–227.

COLEMAN, A. J., SAUNDERS, J. E., CRUM, L. E. & DYSON, M. 1987 Acoustic cavitation generated by an extracorporeal shock wave lithotriper. *Ultrasound Med. Biol.* **13**, 69–76.

DELIUS, M., ENDERS, G., XUAN, Z., LIEBLICH, H. G. & BRENDEL, W. 1988 Biological effects of shock waves: kidney damage by shock waves in dogs – dose dependence. *Ultrasound Med. Biol.* **14**, 117–122.

DOCCHIO, F., REGONDI, P., CAPON, M. R. C. & MELLERIO, J. 1988 Study of the temporal and spatial dynamics of plasmas induced in liquids by nanosecond Nd:YAG laser pulses. 1: Analysis of the plasma starting times. *Appl. Optics* **27**, 3661–3667.

GIOVANNESCHI-TESTUD, P. 1987 Contribution à l'étude de la cavitation à bulles isolées initiées par un rayonnement laser de grande intensité. Thèse d'Etat, Université d'Aix-Marseille II.

HAMMITT, F. G. 1966 Damage to solids caused by cavitation. *Proc. R. Soc. Lond* A **260**, 243–255.

HAMMITT, F. G. 1980 *Cavitation and Multiphase Flow Phenomena.* McGraw-Hill.

HARRISON, M. 1952 An experimental study of single bubble cavitation noise. *J. Acoust. Soc. Am.* **24**, 776–782.

HENTSCHEL, W. & LAUTERBORN, W. 1982 Acoustic emission of single laser-produced cavitation bubbles and their dynamics. *Appl. Sci. Res.* **38**, 225–230.

HERNANDEZ-AVILA, J. L., BONIFACI, N. & DENAT, A. 1994 Hot electron phenomena in liquid and gaseous Ar and N_2 in divergent electric fields. *IEEE Trans. Dielectrics* **1**, 412–418.

HU, C. L. 1969 Spherical model of an acoustical wave generated by rapid laser heating in a liquid. *J. Acoust. Soc. Am.* **46**, 728–736.

KATTAN, R. 1990 Etude de la formation et de la dynamique de bulles dans les hydrocarbures liquides generées par les impulsions de courant en champ électrique intense. Doctoral thesis, Grenoble.

KATTAN, R., DENAT, A. & BONIFACI, N. 1991 Formation of vapour bubbles in non-polar liquids initiated by current pulses. *IEEE Trans. Electr. Insul.* **26**, 656–662.

KATTAN, R., DENAT, A. & LESAINT, O. 1989 Generation, growth and collapse of vapour bubbles in hydrocarbon liquids under a high divergent electric field. *J. Appl. Phys.* **66**, 4062–4066.

KIRKWOOD, J. G. & BETHE, H. A. 1942 Basic propagation theory. In *The Pressure Wave Produced by an Underwater Explosion* (ed. J. G. Kirkwood, E. Montroll, J. M. Richardson, S. R. Brinkley, O. K. Rice & R. Ginell), pp. 588–675. OSRD.

KITAYAMA, O., ISE, H., SATO, T. & TAKAYAMA, K. 1987 Non-invasive gallstone disintegration by underwater shock focusing. *Proc. 16th Intl Symp. on Shock Tubes and Waves, Aachen*, pp. 897–903.

KNAPP, R. T., DAILY, J. W. & HAMMITT, F. G. 1970 *Cavitation.* McGraw-Hill.

LAUTERBORN, W. 1972 High speed photography of laser-induced breakdown in liquids. *Appl. Phys. Lett.* **21**, 27–30.

LEIGHTON, T. G. 1994 *The Acoustic Bubble.* Academic Press.

MCCLUSKEY, F. M. J. & DENAT, A. 1996 The behaviour of bubbles generated by electrical current impulses over a wide range of applied pressures. *J. Appl. Phys.* **80**, 2049–2059.

NAUDE, C. F. & ELLIS, A. T. 1961 On the mechanism of cavitation damage to non-hemispherical cavities collapsing in contact with a solid boundary. *Trans. ASME* D: *J. Basic Engng* **83**, 648–654.

NIGMATULIN, R. I., KHABEEV, N. S. & NAGIEV, F. B. 1981 Dynamics, heat and mass transfer of vapour–gas bubbles in a liquid. *Intl J. Heat Mass Transfer.*, **24**, 1033–1044.

NOACK, J. & VOGEL, A. 1995 Streak-photographic investigation of shock wave emission after laser-induced plasma formation in water. *Laser–Tissue Interactions IV. SPIE Proc.* 2391 (in press).

OSBORNE, M. F. M. & TAYLOR, A. H. 1946 Non-linear propagation of underwater shock waves. *Phys. Rev.* **70**, 322–328.

PEARSALL, I. S. 1972 *Cavitation.* Mills and Boon Ltd.

PHILIPP, A., DELIUS, M., SCHEFFCZYK, C., VOGEL, A. & LAUTERBORN, W. 1993 Interaction of lithotripter-generated shock waves with air bubbles. *J. Acoust. Soc. Am.* **93**, 2496–2509.

PROSPERETTI, A. 1991 The thermal behaviour of oscillating gas bubbles. *J. Fluid Mech.* **222**, 587–616.

RAYLEIGH, LORD 1917 On the pressure developed in a liquid during the collapse of a spherical cavity. *Phil. Mag.* **34**, 94–98.

SACCHI, C. A. 1991 Laser-induced electric breakdown in water. *J. Opt. Soc. Am.* B **8**, 337–345.

VAKIL, N., GRACEWSKI, S. M. & EVERBACH, E. C. 1991 Relationship to model stone properties to fragmentation mechanisms during lithotripsy. *J. Lithotripsy and Stone Disease* **3**, 304–310.

VOGEL, A. & LAUTERBORN, W. 1988 Acoustic transient generation by laser-produced cavitation bubbles near solid boundaries. *J. Acoust. Soc. Am.* **84**, 719–731.

VOGEL, A., LAUTERBORN, W. & TIMM, R. 1989 Optical and acoustic investigations of the dynamics of laser-produced cavitation bubbles near a solid boundary. *J. Fluid Mech.* **208**, 299–338.

WATSON, P. K., CHADBAND, W. G. & SADEGHZADEH-ARAGHI, M. 1991 The role of electrostatic and hydrodynamic forces in the negative point breakdown of liquid dielectrics. *IEEE Trans. Electr. Insul.* **26**, 543–559.

WHEELER, W. H. 1960 Indentation of metals by cavitation. *Trans. ASME* D: *J. Basic Engng* **82**, 184–194.

ZEL'DOVICH, Y. B. & RAIZER, Y. P. 1966 *Physics of Shock Waves and High Temperature Hydrodynamic Phenomena.* Academic Press.